Eur. Phys. J. C (2018) 78:1020
https://doi.org/10.1140/epjc/s10052-018-6489-2

THE EUROPEAN PHYSICAL JOURNAL C

Regular Article - Theoretical Physics

The ultraviolet landscape of two-Higgs doublet models

Manuel E. Krauss[1,a], **Toby Opferkuch**[2,b], **Florian Staub**[3,4,c]

[1] Bethe Center for Theoretical Physics and Physikalisches Institut derUniversität Bonn, Nußallee 12, 53115 Bonn, Germany
[2] PRISMA Cluster of Excellence and Mainz Institute for Theoretical Physics, Johannes Gutenberg-Universität Mainz, 55099 Mainz, Germany
[3] Institute for Theoretical Physics (ITP), Karlsruhe Institute of Technology, Engesserstraße 7, 76128 Karlsruhe, Germany
[4] Institute for Nuclear Physics (IKP), Karlsruhe Institute of Technology, Hermann-von-Helmholtz-Platz 1, 76344 Eggenstein-Leopoldshafen, Germany

Received: 1 August 2018 / Accepted: 30 November 2018 / Published online: 17 December 2018

Abstract We study the predictions of generic ultraviolet completions of two-Higgs doublet models. We assume that at the matching scale between the two-Higgs doublet model and an ultraviolet complete theory – which can be anywhere between the TeV and the Planck scale – arbitrary but perturbative values for the quartic couplings are present. We evaluate the couplings down from the matching scale to the weak scale and study the predictions for the scalar mass spectrum. In particular, we show the importance of radiative corrections which are essential for both an accurate Higgs mass calculation as well as determining the stability of the electroweak vacuum. We study the relation between the mass splitting of the heavy Higgs states and the size of the quartic couplings at the matching scale, finding that only a small class of models exhibit sizeable mass splittings between the heavy scalars at the weak scale. Moreover, we find a clear correlation between the maximal size of the couplings and the considered matching scale.

1 Introduction

Nowadays, there is hardly any doubt that the particle discovered at the LHC in 2012 with a mass of 125 GeV [1,2] is the Higgs boson necessary for electroweak symmetry breaking (EWSB). Although all measured properties of this particle are in good agreement with the predictions of the Standard Model (SM) [3,4], it is nevertheless much too early to abandon the possibility that it is only *one* of *several* Higgs scalars at the weak scale. It is therefore crucial to study the properties and predictions of models with extended Higgs sectors. Two-Higgs doublet models (THDMs) are the next-to-minimal extension of the SM Higgs sector, beyond the minimal extension introducing pure gauge singlet scalars. This additional ingredient can be used to study a wide range of effects: deviations in the couplings of the 125 GeV scalar, the presence of additional neutral Higgs scalars (including the possibility of a state lighter than the SM-like one), new effects mediated by charged Higgs bosons, amongst many other new effects not present in the SM. See for instance Ref. [5] for a detailed overview of these types of models and their phenomenological implications. On the other hand, THDMs address hardly any of the open questions of the SM. For instance both the hierarchy problem and the mechanism responsible for neutrino masses remain unresolved in minimal THDM realizations. THDMs however, are able to accommodate electroweak baryogenesis, providing new sources of CP-violation as well as a modification of the electroweak phase transition to be first-order [6–11]. Modifying the electroweak phase transition requires that one or more of the heavy Higgs masses lie near the SM Higgs mass. However, experimental constraints place lower bounds on the charged Higgs masses, hence a split spectrum implying large quartic couplings is required to realise electroweak baryogenesis [12–16]. Nevertheless, it is likely that – if they indeed turn out to be favoured by experiment at some point – they are only the low-energy limit of a more fundamental theory, such as supersymmetry (SUSY) or a grand unified theory.

Given the large array of possibilities, it is unclear what the ultraviolet (UV) completion of a given THDM might be and at which scale the additional degrees of freedom become relevant. In such a setting, the measurement of a new scalar resonance can shed light on the nature of the UV completion. This expectation arises as THDMs include new renormalisable operators that are therefore unsuppressed by the new physics scale unlike higher dimensional operators induced via new physics. Conversely the absence of any new reso-

[a] e-mail: mkrauss@th.physik.uni-bonn.de
[b] e-mail: opferkuch@uni-mainz.de
[c] e-mail: florian.staub@kit.edu

nances beyond the SM-like Higgs constrains the space of possible UV completions. There are many studies exploring this avenue via a bottom-up approach, i.e. it is assumed that all properties of a THDM at the weak scale are known and it is checked at which energy scale the theory becomes strongly interacting or suffers from an unstable vacuum [17–22]. Assuming that the fundamental UV theory is weakly interacting at all energies, this then indicates the highest possible scale at which new physics is required. In contrast, there are also studies which use a top-down approach: a specific UV model, usually the simplest realisation of supersymmetry, is assumed and the matching conditions to the THDM are calculated [23–26]. These couplings are then evolved down to the low scale where one then checks if what is predicted is in agreement with current measurements. However, the minimal supersymmetric Standard Model (MSSM) as a UV completion for THDMs is peculiar as it predicts that the quartic couplings of the THDM at the matching scale are always small because in the MSSM they are necessarily proportional to the square of the gauge couplings.

Both approaches therefore consider the involved parameters of the theory to be in a very narrow window at the high scale – either they are so large that a perturbative treatment cannot be trusted any more after this point, or they obey special relations, relegating the quartic couplings to comparatively tiny values. A generic UV completion might, however, look very different in the sense that the Lagrangian parameters can take a much larger variety of values. Examples include non-minimal supersymmetric models like the next-to-minimal supersymmetric SM or composite Higgs models, see e.g. Refs. [27,28].

In this work, we utilise a top-down approach, but generalise it to a diverse array of UV completions. Hence, we do not make any assumption about the fundamental theory, but allow for arbitrary couplings at the matching scale. The only requirements on the couplings are that they satisfy perturbativity and perturbative unitarity. To obtain reliable predictions for weak scale physics, we perform a state-of-the-art analysis using two-loop renormalisation group equations (RGEs) and a two-loop calculation of the scalar masses. Moreover, the stability of the electroweak vacuum is checked at the one-loop level in contrast to the common approach to rely on tree-level conditions [29]. Two-loop RGEs have been applied in earlier works on the high-scale behaviour of THDMs [21]. However, they were never previously combined with a matching of the couplings at the loop-level. While one naively expects that the best approach would be to apply one-loop matching when using two-loop RGEs, it has recently been pointed out that this is not the case [30]: when performing N-loop running of the parameters, N-loop matching is required to determine all finite non-logarithmic contributions correctly. This is particularly important in the presence of large couplings, which one often faces in THDMs. Therefore, we find sizeable deviations in the relations between the low- and the high-scale compared to previous studies which only applied a tree-level matching in the bottom-up approach [17–22,31–34]. This difference is especially pronounced when comparing individual parameter points instead of averaging over the properties of a large set of points.

This paper is organised at follows: in Sect. 2 we fix our conventions for the THDM and define our Ansatz to parametrise the high scale theory. In Sect. 3 we discuss the results, pointing out differences and shortcomings of previous approaches, before we conclude in Sect. 4. In the appendix, we provide details about the calculation of the mass spectrum at loop level.

2 The model and the procedure

2.1 The CP-conserving THDM

The scalar potential of the CP-conserving THDM reads

$$\begin{aligned} V = {} & m_1^2 \Phi_1^\dagger \Phi_1 + m_2^2 \Phi_2^\dagger \Phi_2 + \lambda_1 (\Phi_1^\dagger \Phi_1)^2 + \lambda_2 (\Phi_2^\dagger \Phi_2)^2 \\ & + \lambda_3 (\Phi_1^\dagger \Phi_1)(\Phi_2^\dagger \Phi_2) + \lambda_4 (\Phi_2^\dagger \Phi_1)(\Phi_1^\dagger \Phi_2) \\ & + M_{12}^2 (\Phi_1^\dagger \Phi_2 + \Phi_2^\dagger \Phi_1) + \frac{\lambda_5}{2} \left((\Phi_2^\dagger \Phi_1)^2 + (\Phi_1^\dagger \Phi_2)^2 \right) . \end{aligned} \tag{1}$$

Taking M_{12} and λ_5 real ensures CP conservation in the scalar sector. Here we have assumed a $\mathbb{Z}_2$ symmetry which is softly broken by M_{12}^2.[1] Further note that we have defined all parameters in (1) to appear with a positive sign in the potential, i.e. our sign choice for M_{12}^2 differs from most definitions in the literature.

After EWSB, the scalar fields can be written as

$$\Phi_k = \begin{pmatrix} \phi_k^+ \\ \frac{1}{\sqrt{2}} (v_k + \phi_k^0 + i\, \sigma_k) \end{pmatrix}, \quad i = 1, 2. \tag{2}$$

The vacuum expectation values (VEVs) v_i have to fulfil $v_1^2 + v_2^2 = v^2 \simeq (246\,\text{GeV})^2$, and we define their ratio as $\tan\beta = v_2/v_1$. The CP-even neutral scalar fields ϕ_i^0 mix to form the two mass eigenstates h and H where we will always consider the lighter of these states, denoted h, to be the SM-like Higgs discovered at the LHC. The mixing angle which rotates the gauge into the mass eigenstates is commonly denoted as α. The CP-odd states mix to form the physical pseudo-scalar field A as well as the longitudinal component of the Z-boson, while the two charged states form

[1] We assume that the UV completion also respects the Z_2 symmetry at least at tree-level, i.e. the additional couplings $\lambda_6 |H_1|^2 (H_1^\dagger H_2)$ and $\lambda_7 |H_2|^2 (H_1^\dagger H_2)$ are at most loop induced like in the MSSM and will be neglected in this study.

a charged Higgs $H^\pm$ and the longitudinal component of the W boson. The pseudo-scalar as well as the charged Higgs mass matrix are diagonalised by a rotation of the angle β. There are therefore four physical masses and two angles in the scalar sector of the THDM. Out of the eight Lagrangian parameters in (1), m_1^2 and m_2^2 are determined such as to ensure that one is correctly expanding around the minimum of the potential which features the correct pattern of EWSB.

If the THDM is studied only at the low scale, the quartic couplings can be treated as free parameters. Therefore, most of the time in the literature, the five dimensionless parameters λ_i are traded for the four masses m_h, m_H, m_A and $m_{H^\pm}$ as well as the Higgs mixing angle α, whereas the soft $\mathbb{Z}_2$ breaking is directly controlled by choosing M_{12}^2. The relations between the physical tree-level observables and the quartic couplings for our conventions in (1) read [30]

$$\lambda_1 = \frac{1+t_\beta^2}{2(1+t_\alpha^2)v^2}\left(m_h^2 t_\alpha^2 + m_H^2 + M_{12}^2 t_\beta (1+t_\alpha^2)\right), \tag{3}$$

$$\lambda_2 = \frac{M_{12}^2(1+t_\beta^2)}{2t_\beta^3 v^2} + \frac{(1+t_\beta^2)\left(m_h^2 + m_H^2 t_\alpha^2\right)}{2t_\beta^2(1+t_\alpha^2)v^2}, \tag{4}$$

$$\lambda_3 = \frac{1}{(1+t_\alpha^2)t_\beta v^2}\Big[\left(m_H^2 - m_h^2\right) t_\alpha (1+t_\beta^2) + 2m_{H^\pm}^2(1+t_\alpha^2)t_\beta + M_{12}^2(1+t_\alpha^2)(1+t_\beta^2)\Big], \tag{5}$$

$$\lambda_4 = \frac{1}{t_\beta v^2}\left(-M_{12}^2(1+t_\beta^2) + m_A^2 t_\beta - 2m_{H^\pm}^2 t_\beta\right), \tag{6}$$

$$\lambda_5 = \frac{1}{t_\beta v^2}\left(-M_{12}^2(1+t_\beta^2) - m_A^2 t_\beta\right), \tag{7}$$

where $t_x = \tan x$. The advantage of this translation is obvious: interesting parameter regions can directly be defined by the properties of the spectrum and one doesn't have to deal with the Lagrangian parameters directly. Of course, one needs to take care that the implicitly assumed Lagrangian parameters are sensible and do not violate unitarity, for instance.[2] However, this is not possible if the THDM is embedded in a more complete framework as we assume here: in that case the quartic couplings are no longer free parameters but are predicted at the matching scale between the THDM and its UV completion – i.e., there is no direct handle any longer on the masses and mixing angles. Instead, they are predictions at the low scale, to be computed from the running of the couplings while taking care of higher-order corrections.[3] This is completely analogous to the approach in studying constrained versions of SUSY models assuming specific SUSY-breaking mechanisms.

The Yukawa sector of the model is in principle only a doubling of the SM Yukawa sector in that every one of the two Higgs doublets can couple to quarks and leptons:

$$\mathcal{L}_Y = -\bar{L}_L(Y_1^e\Phi_1 + Y_2^e\Phi_2)e_R - \bar{Q}_L(Y_1^d\Phi_1 + Y_2^d\Phi_2)d_R + \bar{Q}_L(Y_1^u i\sigma_2\Phi_1^* + Y_2^u i\sigma_2\Phi_2^*)u_R + \text{h.c.} \tag{8}$$

Here we have suppressed flavour and colour indices. Q_L and L_L are the SM quark and lepton doublets, and d_R, u_R and e_R are the right-chiral down- and up-type quarks as well as the right-chiral charged leptons. The different types of THDMs are distinguished depending on which Yukawa couplings are non-zero. In what follows we consider only two of the most commonly studied types. They are defined as:

- *Type-I* Fermions only couple to the second Higgs doublet, i.e. $Y_1^a = 0 \;\forall\, a = d, u, e$,
- *Type-II* Down-type fermions couple to Φ_1, up-type fermions to Φ_2, i.e. $Y_1^u = Y_2^d = Y_2^e = 0$.

Our main results will also hold for the other cases like Type-III or lepton-specific as long as $\tan\beta$ is small. In this case, the top Yukawa coupling is the only large Yukawa coupling and hence has the largest impact on the running of the model parameters and the loop corrections.

2.2 From the matching scale downwards

Common examples for a UV theory whose low-energy realization is a THDM are for instance high-scale SUSY models with an intermediate m_A. The tree-level matching conditions in this case would be [36]

$$\lambda_1 = \lambda_2 = \frac{1}{8}\left(g_1^2 + g_2^2\right), \qquad \lambda_3 = \frac{1}{4}\left(g_1^2 - g_2^2\right),$$
$$\lambda_4 = -\frac{1}{2}g_2^2, \qquad \lambda_5 = 0. \tag{9}$$

It is well known that higher order corrections are important and therefore, the full one-loop as well as dominant two-loop corrections to these matching conditions have been calculated. Still, these corrections don't change the overall magnitude of quartics at the matching scale, i.e. they are still weak couplings with an absolute size smaller than one. This conclusion does, however, in general not hold for other possible UV completions of the THDM which can lead to much

[2] It has recently been pointed out that for a reliable check of perturbative unitarity in THDMs, the contributions from finite scattering energies s should also be included which were widely ignored before [35].

[3] These loop corrections necessarily spoil the relations Eqs. (3)–(7) which are only valid at tree-level or in an on-shell renormalisation scheme. In order to get a connection to the high-scale when working in an on-shell scheme, one needs to calculate the counter-terms $\delta\lambda$ in order to extract the $\overline{\text{MS}}$ couplings including higher order corrections. These corrected parameters then need to be used in the RGEs when running up in scale [30].

larger values for the quartics. In fact, departing from the idea that minimal SUSY must be the fundamental theory behind the THDM, the model parameters could in principle assume any size depending on the details of the UV completion. As a concrete example consider a singlet-extended MSSM. In contrast to the most general case, some couplings could be forbidden by an R-symmetry for the Higgs and singlet fields. For instance, choosing R-charges of 1 for the Higgs doublets, and zero for the singlet, the following superpotential and soft SUSY-breaking terms are allowed:

$$W = \lambda \hat{S} \hat{H}_d \hat{H}_u + \mu \hat{H}_d \hat{H}_u + W_Y \tag{10}$$

$$-\mathcal{L}_{\text{SB}} - \mathcal{L}_{\text{SB},\tilde{f}} = m_{H_d}^2 |H_d|^2 + m_{H_u}^2 |H_u|^2 + m_S^2 |S|^2 + B_S S^2 + T_\kappa S^3 + LS + \text{c.c.} \tag{11}$$

where W_Y contains the superpotential terms with Yukawa couplings as in the MSSM and $\mathcal{L}_{\text{SB},\tilde{f}}$ summarises all soft SUSY-breaking terms involving sfermions. $\hat{H}_u$ and $\hat{H}_d$ are the Higgs superfields of a type-II THDM while $\hat{S}$ is a SM gauge singlet superfield. The unhatted fields refer to the scalar component of the superfield in question. If we neglect all contributions from VEVs, the matching conditions at tree level between this model and the THDM become [37]

$$\lambda_1 = \lambda_2 = \frac{1}{8}\left(g_1^2 + g_2^2 + \frac{4\sqrt{2}\lambda^2\mu^2}{M^2}\right), \tag{12}$$

$$\lambda_3 = \frac{1}{4}\left(-g_1^2 + g_2^2 + \frac{12\sqrt{2}\lambda^2\mu^2}{M^2}\right), \tag{13}$$

$$\lambda_4 = -\frac{1}{2}g_2^2 + \lambda^2, \tag{14}$$

$$\lambda_5 = 0, \tag{15}$$

where $M = \frac{1}{2v_S}\left(\sqrt{2}v_S^2 T_\kappa - 2\sqrt{2}L\right)$ is the mass of the heavy CP-even singlet. Since λ is now a free parameter, one can generate much larger values for the quartics of the THDM at tree level. Of course, in this set-up some correlations between the quartics would still exist because they depend on some fundamental parameters. However, this would also change in even more complicated UV models, especially in non-supersymmetric scenarios where the restrictions on the form of the scalar potential are much weaker.

Therefore, we are interested in the much more general case and assume that all (perturbative) values of the quartic couplings are allowed at the matching scale Λ, i.e. they can be in the range

$$\lambda_i(\Lambda) \in [-4\pi, 4\pi], \tag{16}$$

while also satisfying the perturbative unitarity constraints [38,39]. Even if we allow in principle for this large range of couplings, we will see that the phenomenologically relevant parameter space is much smaller. Above the matching scale we don't demand that the couplings are perturbative, i.e. we allow also for strongly coupled UV completions.

2.3 Calculating the mass spectrum

Our goal is to assess the relations between the electroweak (or TeV) scale and a higher scale where the quartic couplings are predicted from matching them to the UV theory. As such, it is necessary to treat the couplings as $\overline{\text{MS}}$ parameters (rather than applying an on-shell scheme) which are then evolved down to the low scale where the spectrum is calculated. In summary, the following steps have to be performed:

1. Fix the ($\overline{\text{MS}}$) couplings at the matching scale Λ.
2. Evolve the couplings down to the weak scale. For that, we are using the full two-loop RGEs.
3. Calculate the scalar masses and mixing angles including the higher order corrections to the spectrum. In the neutral scalar sector, we compute the full one-loop corrections and add the most important two-loop pieces in the limit of vanishing external momenta. The charged Higgs is calculated at the full one-loop level.

In Appendix A, we provide additional details of the procedure used. The urgent need to go to the two-loop level in order to get a reliable prediction for the Higgs mass in the presence of large quartic couplings is demonstrated in Fig. 1 where we show the dependence of the calculated mass on the chosen renormalisation scale for moderately large quartic couplings. In this example, we use the running quartic couplings as input at the top mass scale and evolve them up to the scale Q where we perform the mass renormalisation. The change in the Higgs mass prediction by varying the renormalisation scale can be used as an estimate of the theoretical uncertainty at the different loop-levels. It is seen that, while the scale dependence is huge in the case of a tree-level calculation, the inclusion of the one- and two-loop mass corrections reduces this dependence heavily. Only by including the two-loop corrections we can assume that the theoretical uncertainty is in the ballpark of a few GeV.

Finally we note that the usage of the full two-loop RGEs is, in addition to the radiative Higgs mass corrections, crucial for the accuracy of the predictions when running from the matching scale down to the top mass scale since there can be sizeable differences between the one- and two-loop running. In order to demonstrate this, we have chosen the quartic couplings as input at a matching scale of $\Lambda = 10^8$ GeV to be

$$\lambda_1(\Lambda) = 2.37, \quad \lambda_2(\Lambda) = 1.21, \quad \lambda_3(\Lambda) = -0.25, \quad \lambda_4(\Lambda) = -1.21, \quad \lambda_5(\Lambda) = 0.71. \tag{17}$$

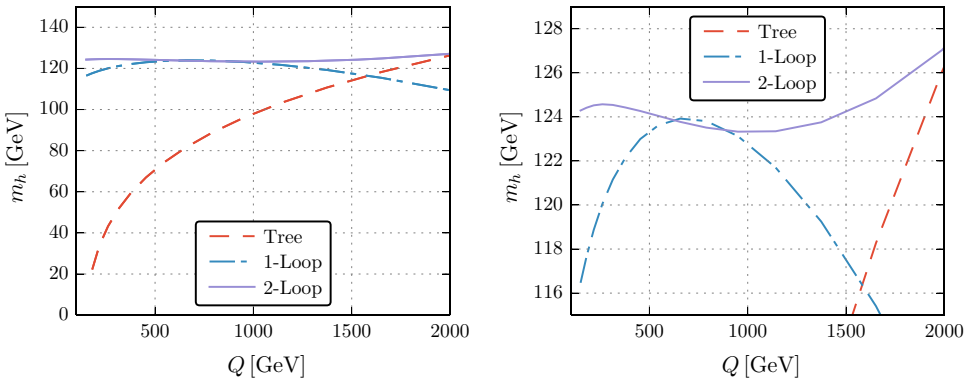

Fig. 1 Estimate of the theoretical uncertainty at a given loop level: the Higgs mass at tree (red), one-loop (blue) and two-loop level (purple) as a function of the renormalisation scale Q. As input, we use the running parameters at the top mass scale and evolve them up to Q. We have used $\lambda_1 = 1.09$, $\lambda_2 = 0.58$, $\lambda_3 = -3.27$, $\lambda_4 = 0.87$, $\lambda_5 = 0.81$, $M_{12} = -750^2$ GeV^2 as well as $\tan\beta = 1.18$. The left-hand panel is a zoomed in version of the right-hand panel, to better illustrate the difference between the 1- and 2-loop computations

The RGE running at the one- and two-loop level is shown in Fig. 2 while the impact on the running quartic couplings as well as the scalar masses is summarised in Table 1.

Here, the change in the light Higgs mass is more than 10 GeV, even with this choice of moderately large quartics at the matching scale. For extreme cases where these couplings approach the limit of 4π, the effects can be much more extreme: points which behave well with two-loop RGEs easily seem to predict tachyonic states at the weak scale if only one-loop RGEs would have been used.

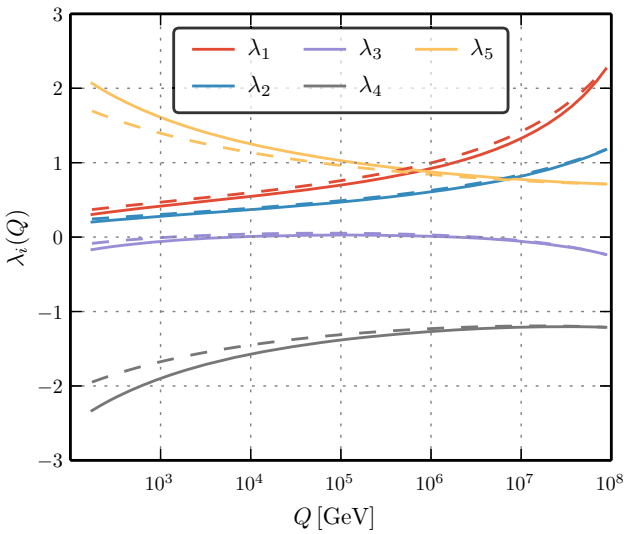

Fig. 2 The RGE running at one-loop (dashed) and two-loop (full) of the quartic couplings λ_i when fixing the values at the matching scale of $\Lambda = 10^8$ GeV according to (17)

3 Results

3.1 Numerical set-up and constraints

3.1.1 Mass spectrum calculation

For the numerical calculations we make use of the `Mathematica` package `SARAH` [40–45] to produce a spectrum generator based on `SPheno` [46–48]. As outlined in Appendix A, the spectrum is calculated in the $\overline{\text{MS}}$ scheme at the full one-loop order including all important two-loop corrections for the neutral scalars [49–51]. We have modified the one-loop calculation in such a way that it includes the analytic continuation of loop functions for negative squared masses as input. This is necessary as the one- and two-loop corrections to the SM-like Higgs are often so large that only a negative mass squared at tree-level would lead to a phenomenologically viable spectrum at the two-loop order, otherwise one clearly overshoots the required mass of 125 GeV. While it might be uncommon to start with a tachyonic tree-level spectrum, one can think of this as a situation where the expansion around the electroweak VEV is a bad one at tree level while the minimum at the right place only emerges at the loop order.[4] On the other hand, this issue can be regarded as an artefact of using an $\overline{\text{MS}}$ scheme. While both the $\overline{\text{MS}}$ and on-shell scheme are viable prescriptions to calculate the spectrum, only the on-shell scheme enforces the correct minimum of the potential at every loop order. In $\overline{\text{MS}}$ the tree-level masses can be very different, i.e. this minimum does not have to be present at every order of perturbation theory, but it has to exist at the highest loop order.

[4] In some specific supersymmetric models, the only way to obtain a phenomenologically viable spectrum is actually to start with a tachyonic tree-level spectrum which turns into a consistent spectrum at the bottom of a (potentially global) electroweak minimum appearing only at the loop level. See for instance Refs. [52,53].

Table 1 The running quartics at the one- and two-loop level for the input given in (17). The given values for the masses correspond to a two-loop calculation using $\tan\beta = 1.4$ and $M_{12} = -500^2$ GeV^2

RGEs	$\lambda_1(m_t)$	$\lambda_2(m_t)$	$\lambda_3(m_t)$	$\lambda_4(m_t)$	$\lambda_5(m_t)$	m_h[GeV]	m_{H^0} [GeV]	m_{A^0} [GeV]	m_{H^+} [GeV]
1-loop	0.304	0.202	−0.168	−2.331	2.067	123.6	749.1	660.4	735.8
2-loop	0.370	0.243	−0.084	−1.948	1.695	111.6	749.4	646.0	736.2

3.1.2 Scanning procedure

If we would start with random values of the quartics as well as M_{12} at the matching scale and evolve them down, this would correspond to a pure 'top-down' approach. However, a parameter scan done in that way would be very inefficient, mainly because the correct Higgs mass of $m_h \simeq 125$ GeV would hardly ever be obtained. Therefore, we use the more practical Ansatz and scan for $\lambda_i(m_t)$ which give the correct Higgs mass at the two-loop level for given values of $\tan\beta$ and M_{12}. These couplings are then evolved up to higher scales using the full two-loop RGEs of the THDM. Here, we are not only interested in the cut-off scale (i.e. the scale where perturbativity or unitarity breaks down) but also all other intermediate scales Λ. This Ansatz is completely equivalent to choosing $\lambda_i(\Lambda)$ and $M_{12}(\Lambda)$ randomly at the high scale and keeping only points which have the correct value for m_h and some desired value for M_{12} at the low scale – with the virtue that we do not have to run the RGEs on points which are being disregarded in the end.

Apart from the quartic couplings, the remaining free model parameters are the soft $\mathbb{Z}_2$-breaking term M_{12}^2 as well as the VEV ratio $\tan\beta$. For M_{12}^2, we choose values between $-M_{12}^2 = [0, (1\text{ TeV})^2]$ at the weak scale while for $\tan\beta$ we choose values between 1 and 2. We have confirmed, by extending the range of chosen $\tan\beta$ values, that the $\tan\beta$ dependence of our results is negligible compared to the impact of λ_i and M_{12}.

3.1.3 Theoretical constraints

We place several conditions on the resulting parameter points. First, as mentioned earlier, we apply the unitarity conditions [38,39]. For this we use the quartic couplings entering the two-loop mass spectrum calculation. Therefore the resulting unitarity constraints, when translated to the physical masses, differ w.r.t. the typical tree-level considerations. Note that this approach is the $\overline{\text{MS}}$ analogue of using the shifted couplings in an on-shell scheme as proposed in Ref. [54]. We enforce convergence of the perturbative series by demanding that the two-loop correction to all scalar masses has to be smaller than the one-loop corrections, $|(m_\phi^2)^{\text{2L}} - (m_\phi^2)^{\text{1L}}| < |(m_\phi^2)^{\text{Tree}} - (m_\phi^2)^{\text{1L}}|$, with $\phi = h, H, A$ [51,54]. We also apply the conditions for a stable vacuum: Since loop effects in the Higgs sector are crucial it is not reliable to use the common tree-level checks as has been demonstrated in Ref. [55]. Instead, we numerically check the vacuum stability using the tool `Vevacious` [56]. This determines the stability of the one-loop effective potential at the low scale. `Vevacious` makes use of the homotopy continuation method provided with `HOM4PS2` [57] to find all tree-level extrema of the scalar potential. It then includes the one-loop corrections according to Coleman and Weinberg [58] and searches numerically for all minima in the vicinity of the tree-level extrema. We only take parameter points into consideration which feature a stable electroweak vacuum, i.e. we disregard regions of parameter space where the electroweak minimum is the false vacuum. The reason is that the tunnelling to minima with VEV values up to a few TeV is very efficient and always leads to a short-lived electroweak vacuum on cosmological time scales.[5]

3.1.4 Experimental constraints

We also apply the most important experimental constraints. First of all, we demand a SM-like Higgs mass in the range

$$m_h = 125\text{ GeV} \pm 3\text{ GeV}\,. \tag{18}$$

This average uncertainty of 3 GeV in the Higgs mass prediction might be too pessimistic for points with small couplings and too optimistic in the presence of huge λ's. However, we expect no changes in our results using an uncertainty estimate specifically developed for 2HDMs.[6] We furthermore test parameter points against `HiggsBounds` [61,62] to check whether a point is allowed by Higgs coupling measurements. Finally, we impose a lower bound on the charged Higgs mass for the separate cases of type-I and -II Yukawas due to the constraints from $B \to X_s\gamma$ and $B \to X_d\gamma$ [63].

[5] We only consider minima which are 'close' to the electroweak one. In this regime, the fixed-order calculation at the one-loop level gives reliable results. For minima involving much larger VEVs, one must consider the RGE-improved potential, also including potentially large effects from gravity. In addition one would need to carefully estimate the tunnelling rate at finite temperature including also the impact of inflation and reheating which was so far done only for the SM [59]. This is beyond the scope of this paper. Instead, we assume that the vacuum at very high energies can be stabilised by Planck suppressed operators which otherwise do not have any impact on the phenomenological results [60].

[6] We stick to the fixed estimate because it's not even clear in well established models like the NMSSM how a robust and point-dependent uncertainty estimate should be performed.

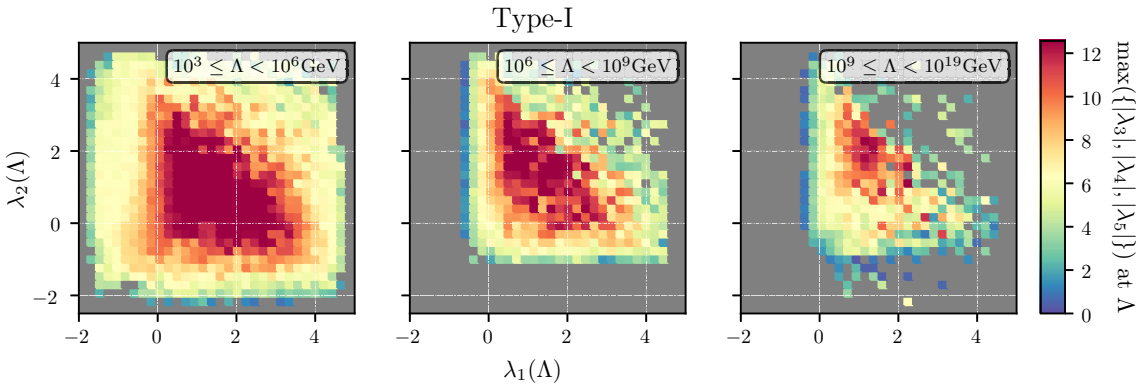

Fig. 3 The per-bin maximal value of $\{|\lambda_3|, |\lambda_4|, |\lambda_5|\}$ as a function of λ_1 and λ_2 at the matching scale. In the plots from left to right, we show three different ranges of the matching scale. We use Yukawa textures of type-I for this figure

Other flavour constraints, which could be included via the `FlavorKit` functionality of `SPheno` [64] are weaker in the considered scenarios.

3.2 Numerical results

We now turn to the discussion of the numerical results. We start with summarising the overall results, i.e. what are the preferred values of the quartic couplings at the matching scale, and how does the physics at the weak scale depend on the couplings and the matching scale. Afterwards, we go into detail and analyse the impact of the included higher order corrections.

3.2.1 The couplings at the matching scale

Since λ_1 and λ_2 are the most important quartic couplings, i.e. they determine the magnitude of the SM-like Higgs mass as well as (tree-level) vacuum stability, it is natural to investigate their possible ranges. Recall in the MSSM $\lambda_1 = \lambda_2 > 0$ while tree-level vacuum stability of THDMs restricts both λ_1 and λ_2 to positive values at the electroweak scale. In Fig. 3, we present the values of λ_1 and λ_2 at the matching scale, divided into three ranges of matching scales: 10^3–10^6 GeV (left), 10^6–10^9 GeV (middle) and 10^9–10^{19} GeV (right). The maximal (positive) values which we find for these two couplings are constrained by perturbative unitarity checks which restrict $\lambda_{1(2)} < 8\pi/6$ if at the same time all other quartic couplings are zero.

Thus, even when allowing for a large range of λ_1 and λ_2 values at the matching scale, we find that physical constraints drastically reduce the allowed range of these two quartics. In particular, large negative values for these couplings remain disfavoured by the stability of the electroweak vacuum even when including higher order corrections. The smallest possible value which we found is about -2 for low matching scales, while for higher matching scales negative λ_1 is hardly possible. Recall that if one were to apply the tree-level conditions for unbounded-from-below (UFB) directions, one would immediately drop all parameters with negative λ_1 and/or λ_2. As a generic result, we also see that large $\lambda_{3,4,5}$ is only allowed at the matching scale if $\lambda_{1,2}$ is moderately large, i.e. $0 \lesssim \lambda_{1,2} \lesssim 3$. The plot on the right-hand side of Fig. 3 which displays the case of large matching scales suggests that the larger the matching scale, the smaller the allowed couplings are. This is actually a non-trivial statement as one one might have expected that the choice of the matching scale can always be compensated by varying the different quartic couplings without changing the overall magnitude of these couplings. These conclusions remain qualitatively unchanged when looking at the average λ_i, while the situation in type-II THDMs is very similar.

3.2.2 The spectrum of THDMs

We turn to the discussion of the scalar mass spectrum. The largest difference between general THDMs and THDMs arising from a UV completion, like the MSSM, is that the mass splitting between the heavy scalars can be very large. In contrast, the THDM matched to the MSSM always predicts that the heavy CP-even and -odd Higgs states are nearly degenerate, and the charged Higgs mass only differs by the W boson mass.

We show in Fig. 4 the maximal mass splitting $\max(\Delta M = |M_i - M_j|)$ (evaluated at m_t), where $i = H^0, A^0, H^\pm$, as a function of the matching scale Λ and the maximal, absolute value of the quartic couplings at that scale. We also show the results for different ranges of M_{12}. One can draw the connection to previous studies using the bottom-up approach and checking for the cut-off scale of the theory by looking at the region of the plot with the largest quartic couplings, while the MSSM-like parameter region corresponds to the area close to the x-axis. In general, we observe that sizeable mass splittings are easier to achieve when matching the THDM to a

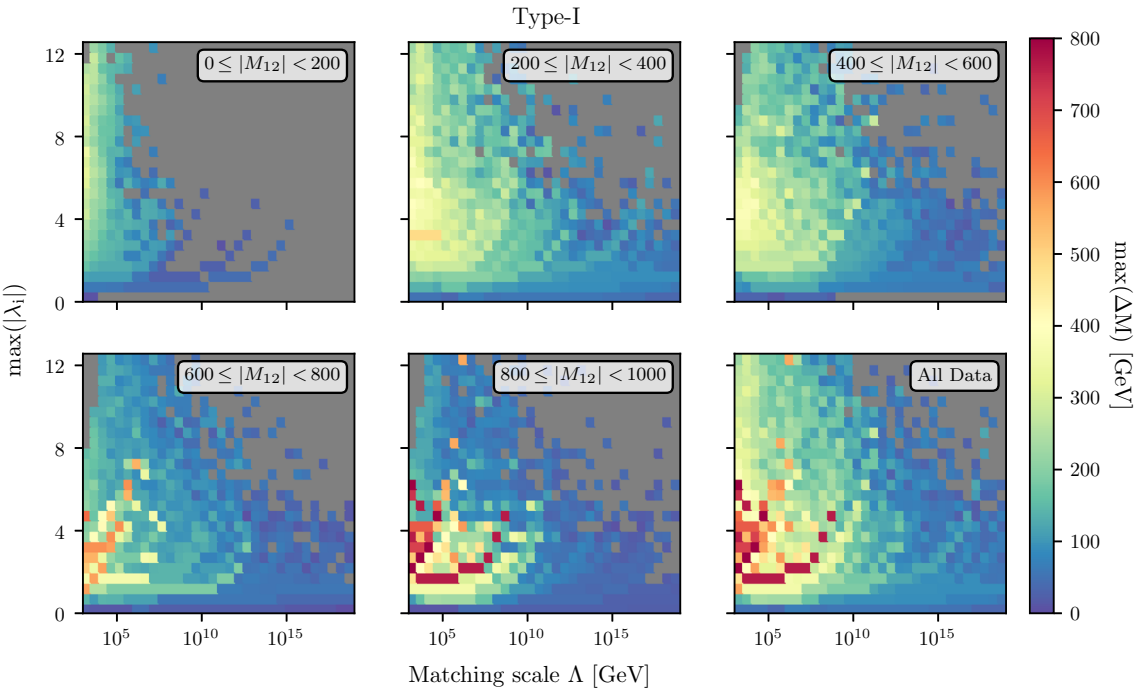

Fig. 4 The maximal mass splitting between the heavy Higgs states ΔM, evaluated at the electroweak scale, as a function of the matching scale Λ and the value of the maximal quartic coupling at Λ. We use the Yukawa scheme of type-I for this figure

UV theory at rather low scales. In particular for matching scales above 10^{10} GeV and $|M_{12}| < 200$ GeV we rarely find points where the mass splitting between different heavy Higgs states at the electroweak scale turns out to be larger than ~ 100 GeV. If, instead, the mass splitting ΔM should be of several hundreds of GeV, then this *can not* be realised with matching scales beyond 100 TeV, particularly so if M_{12} is small. Actually, for this choice of $|M_{12}|$ it is in general difficult to find any valid models at all with large couplings and high matching scale even with small mass splittings in the scalar sector. This statement changes when moving to larger values of M_{12}: already for $|M_{12}| \sim 500$ GeV we can find parameter points which agree with all the electroweak-scale physics while having a matching scale around 10^{10} GeV and mass splittings up to 400 GeV. For larger values of $|M_{12}|$, this situation does not change significantly as can be seen in the lower row of Fig. 4.

The most unexpected feature is the largest mass splittings do not appear for the largest values of quartic couplings at the matching scale, but for moderately large couplings of $\mathcal{O}(2-6)$ and large values of $|M_{12}|$ of $\mathcal{O}(1\,\text{TeV})$. The reason is that for those values of M_{12} larger quartic couplings are forbidden as the corrections to m_h become too large.

Note that while Fig. 4 displays the case of type-I Yukawas, the picture is very similar for type-II, and hence the conclusions are the same. The only difference is that the upper left plot featuring $|M_{12}| < 200$ GeV is not populated in the THDM-II because of the tighter constraints on the charged Higgs mass from B observables.

Interestingly, when looking at the average mass splittings between the heavy scalars, we obtain a different picture, as is shown in Fig. 5. In this figure we show the per-bin averaged ΔM instead of the maximal value per bin as before. We find that, while mass splittings of ~ 150 GeV typically occur for low $|M_{12}|$, $\max(|\lambda_i|) \gtrsim 2$ and matching scales below 10^{10} GeV, this is not any more the case for larger values of $|M_{12}|$ where smaller mass splittings of 50–100 GeV are preferred.

3.2.3 *Impact of scalar loop corrections on the light Higgs*

We now take a closer look at the size of the one- and two-loop mass corrections which we obtain for the SM-like Higgs state. As announced earlier, these are generically quite large. Depending on the matching scale, we consider the radiative correction to the Higgs mass (calculated at the top mass scale) as a function of M_{12}^2 which we define as

$$\Delta m_h = \sqrt{\left| m_h^{2,\text{loop}} - m_h^{2,\text{tree}} \right|}\,. \tag{19}$$

Here we denote $m_h^{2,\text{tree}}$ as the mass which we would obtain when calculating the Higgs mass at tree-level with the quartic couplings that eventually lead to the 125 GeV at two-loop. It is therefore *not* equivalent to the on-shell mass but can be

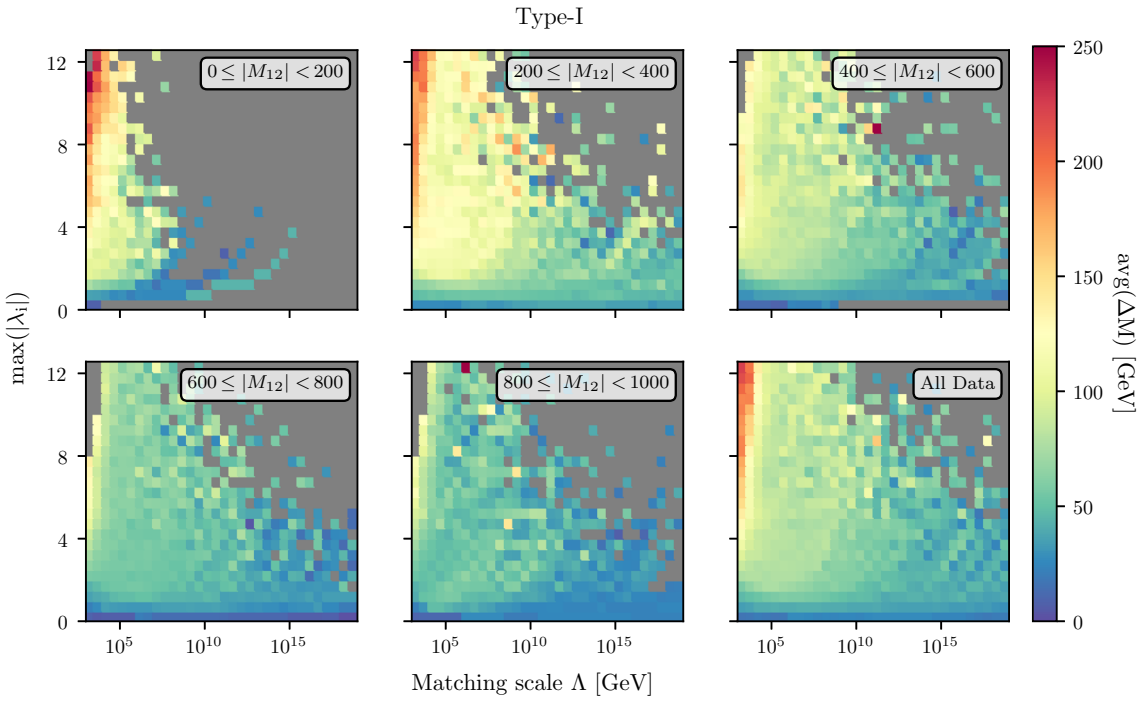

Fig. 5 Same as Fig. 4 but with the per-bin average of ΔM instead of the maximal value

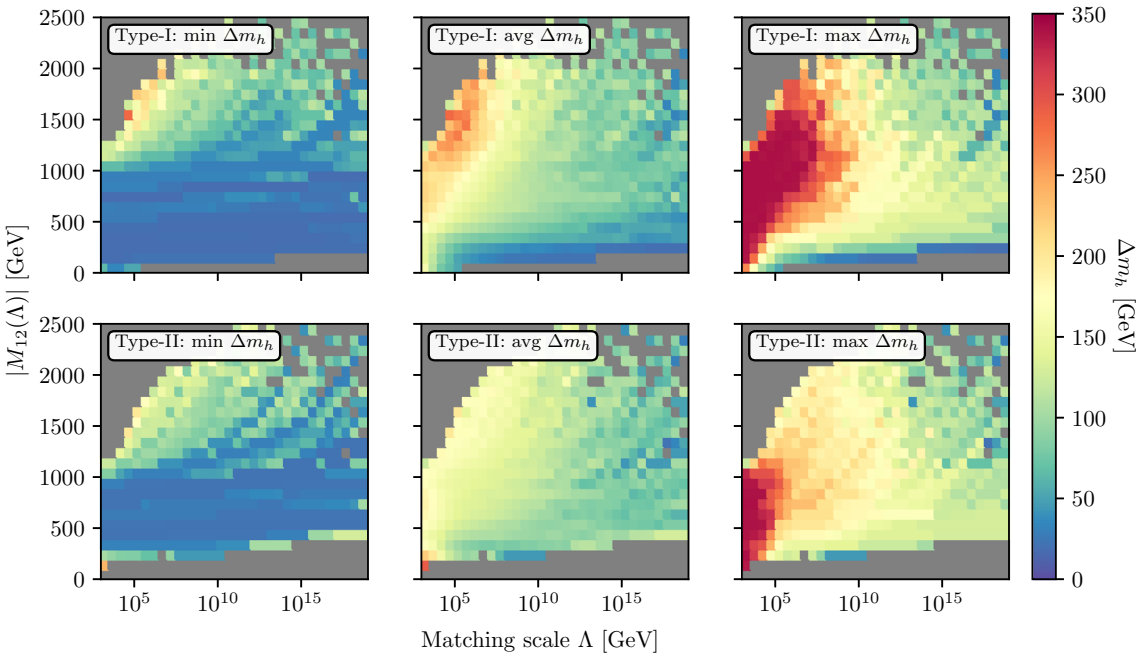

Fig. 6 Size of the loop corrections to m_h as a function of the matching scale Λ and $M_{12}(\Lambda)$. The colours in the plane represent the minimal (left), average (middle) and maximal (right) size of the radiative corrections in the respective bin. We are using type-I Yukawas in the upper row and type-II in the lower row

seen as the input parameter for obtaining the $\overline{\text{MS}}$ λ_i when using Eqs. (3)–(7).

We show the results for the THDM of both type-I (upper row) and type-II (lower row) in Fig. 6 in the two-dimensional plane matching scale vs $|M_{12}(\Lambda)|$ to represent the minimal, maximal and average Higgs mass correction in the respective bin. We see that while the minimal correction is smaller than 100 GeV almost throughout the entire plane, the maximal correction can be as large as 300 GeV for small matching scales. The reason for this behaviour is clear: large

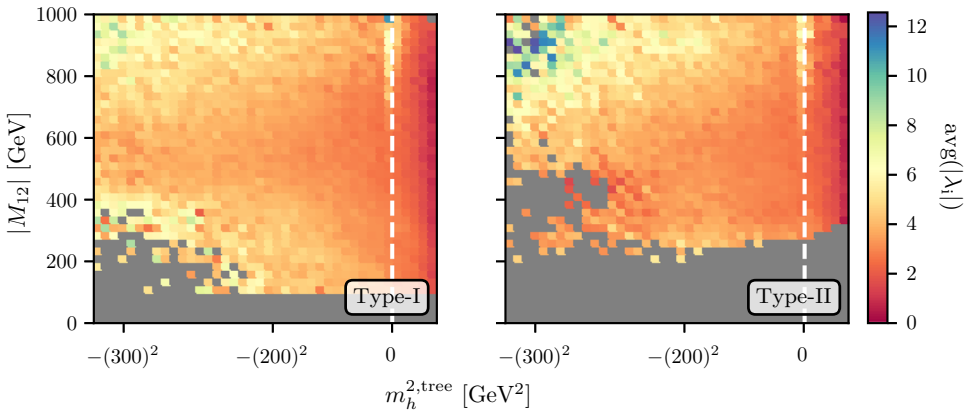

Fig. 7 Size of the average electroweak-scale quartic couplings as a function of the tree-level input mass $m_h^{2,\text{tree}}$ and $|M_{12}|$ using the THDM of type-I (left) and -II (right)

loop corrections are driven by large couplings at the electroweak scale – which are more likely to be obtained with low matching scales as can be seen in the previous figures. Even the averaged radiative corrections to the Higgs mass are $\mathcal{O}(100\text{ GeV})$. This shows that a calculation beyond leading order is absolutely crucial for obtaining sensible predictions. Of course, one might feel uncomfortable by these huge loop corrections and wonder about the validity of the perturbative series. As we have stated above, we applied the condition that the two-loop corrections must always be smaller than the one-loop corrections to filter out the most pathological points. In principle, one can apply even stronger constraints on the size of these loop corrections. This would correspond to disfavouring certain classes of UV completions with very large quartic couplings and might be a conservative approach. We always included these extreme parameter regions in order to stress the necessity to include radiative corrections to the scalar masses in 2HDMs which hasn't been done in literature before.

The main difference between the cases of type-I and type-II Yukawas stem from the more stringent constraints on the latter type [63], leading to a lower bound on $m_{H^\pm_{\text{type-II}}}$ of $\mathcal{O}(600\text{ GeV})$. Since M_{12} sets the overall scale of the heavy Higgs states, this cut constrains a combination of λ_i and M_{12} and therefore leads to larger minimal $|M_{12}|$ values for type-II models.

Finally we want to illustrate the ranges of tree-level input parameters that we have to use in order to achieve a 125 GeV lightest Higgs. As explained in Sec. III A 1, it is necessary to often use negative $m_h^{2,\text{tree}}$ in order to achieve the correct Higgs mass at the two-loop order. In Fig. 7, we present the range which we used for our study. We contrast this against the electroweak-scale $|M_{12}|$ and show the per-bin average of the λ_i in this plane. We observe that valid spectra are only compatible with positive $m_h^{2,\text{tree}}$ if the quartics are moderate, $\lesssim 4$. Couplings beyond this value cause the loop corrections to be so large that negative squared input masses are needed – and the larger the quartic couplings, the more extreme ranges of $m_h^{2,\text{tree}}$ are needed. One can see from these large loop corrections that a tree-level study of the Higgs sector is very unreliable. This also underlines the need to test for vacuum stability at the loop level.

3.2.4 *The sensitivity of the cut-off scale on higher-order corrections*

The size of the loop corrections discussed in the previous subsection can be translated into the shift in cut-off scale, see Ref. [30] for further details. We define this scale as the largest scale up to which a perturbative treatment of the THDM is still justifiable, i.e. as the point at which either one of the quartic couplings becomes larger than 4π or where the perturbative unitarity conditions are not satisfied any more due to the RGE evolution of the λ's.

We show the number of points affected by these considerations in Fig. 8. More specifically we show the cut-off scale when using two-loop Higgs mass corrections at the top mass scale (i.e. a two-loop matching of the THDM to the SM) and two-loop RGE running (denoted (2, 2)) against the cut-off when doing tree-level matching at the weak scale and one-loop running, $(T, 1)$. For the latter, we use Eqs. (3)–(7) in order to obtain the tree-level – or on-shell – couplings from the mass spectrum for each point.

One first obvious observation is that the majority of points accumulate at low cut-off scales below 100 TeV – which is of course no surprise when sampling the parameter space randomly with a flat distribution in the quartics. The second observation is that there is a trend towards higher (2, 2) cut-off scales. This is seen as the deviation from the diagonal white line in Fig. 8 and derives from the fact that the two-loop corrections to the RGEs typically reduce the absolute size of the β-functions and therefore the slope of the running. Although the majority of the points are characterised by this behaviour, it is interesting to see how drastic the change in matching and running can affect the high-scale behaviour of

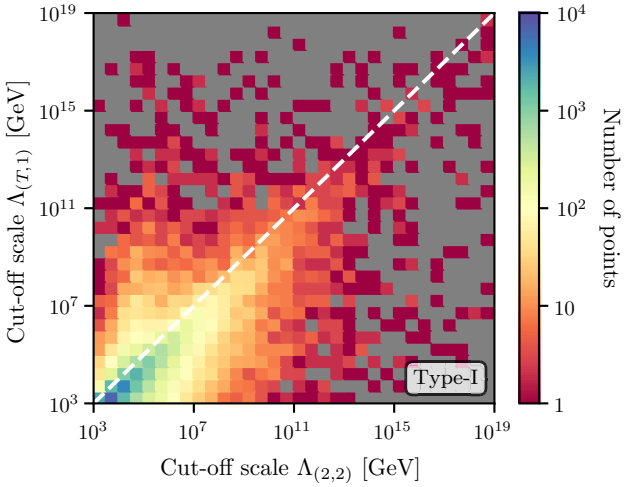

Fig. 8 Number of parameter points depending on the cut-off scale when including two-loop mass corrections and two-loop RGE running (2, 2) as well as when doing a tree-level mass computation and one-loop running $(T, 1)$. Here we have applied the Yukawa scheme of type-I. The white line is the diagonal along $\Lambda_{(T,1)} = \Lambda_{(2,2)}$

a parameter region: we find points where the cut-off scale in the (2, 2) calculation is larger than the $(T, 1)$ prediction by ten orders of magnitude or more – and vice versa. This is a direct consequence of the mostly large one- and two-loop mass corrections to the scalars. The corresponding shift in λ when matching at two-loop compared to matching at tree-level can consequently lead to drastic differences in the high-scale behaviour. In particular, it is worth stressing that the biggest changes appear for large cut-off scales which correspond to at most moderately large quartic couplings at the weak scale. Thus, for these points the perturbative series at the weak scale behaves well and the loop corrections to the quartics are absolutely trustworthy, while the missing higher-order corrections from three-loop contributions and above can be expected to be small. As the distribution of points around the white dashed line in Fig. 8 appears symmetric for larger values of the cut-off, it is tempting to argue that a tree-level mass spectrum calculation in conjunction with one-loop RGEs is sufficient at a statistical level. However, in advocating specific benchmark points, especially for use in experimental searches, it is essential that the complete state-of-the-art calculations be performed to properly ascertain their validity with respect to both theoretical and experimental constraints. Again we note that there are no sizeable differences between the cases of type-I and type-II Yukawa textures.

3.2.5 *Vacuum stability*

Finally we comment on the conditions for electroweak vacuum stability. As discussed earlier, we use the one-loop effective potential in order to find all extrema in the vicinity of the tree-level extrema checking whether there exists a deeper global minimum. We only keep points which feature a stable desired electroweak vacuum configuration. The resulting constraints are in general different from the usual tree-level vacuum stability conditions, see Ref. [55] for more details. In Fig. 9, we show the fraction of parameter points in each bin which passed the one-loop constraints which would also have passed the tree-level vacuum stability conditions. For calculating the tree-level constraints, we again use the tree-level couplings obtained by Eqs. (3)–(7) and calculate the tree-level potential.

In accordance with Ref. [55], we find that large regions of parameter space which feature a perfectly fine EWSB global minimum at the one-loop order would have been regarded unstable by the tree-level checks – meaning that these regions are resurrected by the radiative corrections. While for small $|M_{12}|$, the tree-level conditions would have allowed almost all of the parameter points, it is clearly seen that for larger values of $\mathcal{O}(400\ \text{GeV})$ and higher, far less than half of the points would have been considered allowed when applying the conventional checks. Interestingly, M_{12} is the most decisive factor in the change of tree-level forbidden to loop-level allowed. The size of the quartic couplings instead plays an important though inferior role. In particular, for $|M_{12}| \gtrsim 600\ \text{GeV}$ and $\max(|\lambda_i|)_{\text{EWSB}} \gtrsim 5$ (which is of course exactly the region where the scalar loop corrections are large and therefore also the corrections to the potential), virtually all the parameter space would be ruled out by the tree-level checks – but not so once the radiative corrections are taken into account. The reason for this behaviour can be found in the size of the scalar loop corrections in this region: as discussed earlier, M_{12} drives the (positive) loop corrections to the lightest Higgs mass. As a result, in an $\overline{\text{MS}}$ scheme, we often need *large negative* $\lambda_{1,2}$ in order to obtain the correct Higgs mass at two-loop order. The area in the figure where almost none of the allowed points would have been allowed at the tree level corresponds to exactly this situation. As a matter of fact, although the threshold corrections drive $\lambda_{1,2}$ to quite large negative numbers, their tree-level – or on-shell – equivalents are usually also negative. However, since negative $\lambda_{1,2}$ lead to field directions which are unbounded from below at tree-level [65], the tree-level calculation would result in the statement that these points are excluded. At the loop level, however, the situation is different as the large loop corrections can lift the potential in these unbounded-from-below directions and therefore stabilize the vacuum [55]. Lastly note that the lack of parameter points on the right-hand side (displaying the THDM-II case) for both low $|M_{12}|$ and $|\lambda_i|$ is again due to the stronger cuts on $m_{H^\pm}$ which require either of both to be large in order to produce the large masses needed.

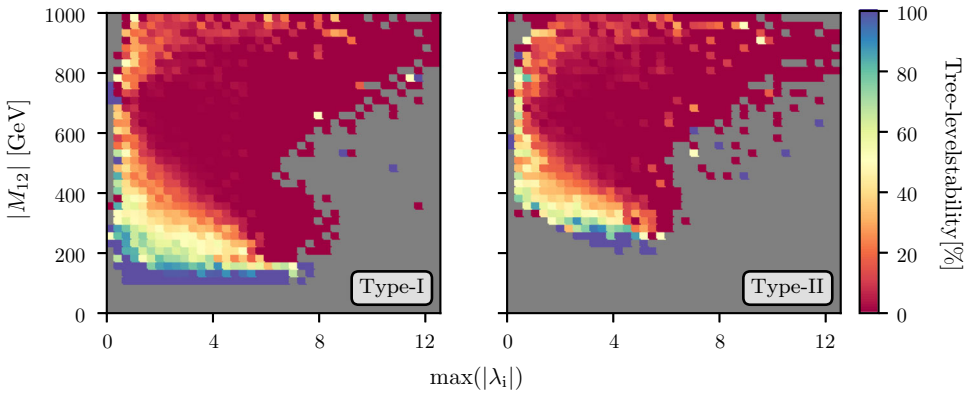

Fig. 9 Per-bin percentage of points that would have survived the one-loop vacuum stability constraints but would not have passed the tree-level conditions, as a function of $|M_{12}|$ and $\max(|\lambda_i|)$, evaluated at the electroweak scale. The left plot shows the case of type-I Yukawas and the right one a Yukawa texture of type-II

4 Summary and conclusions

In this paper, we have studied generic predictions from UV completions of THDMs. We have not specified the particular UV-complete model but rather investigated the low-energy consequences of general boundary conditions at a particular matching scale, i.e. leaving the THDM parameters arbitrary at this scale. By the use of the two-loop renormalisation group equations, those parameters were then evolved down to the electroweak scale where we also applied the two-loop threshold corrections for the Higgs mass. All obtained spectra have then been confronted with the current experimental constraints as well as the vacuum stability considerations. We further demanded perturbativity and perturbative unitarity of the theory everywhere between the TeV and the matching scale. We have seen correlations between the matching scale and the mass splitting ΔM in the heavy Higgs sector at the electroweak scale. As a generic feature, we find that large matching scales near the Planck scale would predict very small ΔM independent of the size of the quartic couplings at the scale. If, in turn, this splitting should be of the order of several hundreds of GeV, this would point to very large couplings at a matching scale not much larger than the TeV scale probed so far at experiments, placing serve constraints on the possibility of realising electroweak baryogenesis in THDMs.

We have highlighted the importance of the loop corrections to the Higgs mass which need to be taken into account for reliable predictions. Likewise, we have shown that an examination of the stability of the electroweak vacuum needs to be done beyond tree level – or else we would wrongly consider many perfectly-allowed regions of parameter space as ruled out.

Acknowledgements We thank Johannes Braathen and Mark D. Goodsell for useful discussions and the LPTHE in Paris for hospitality. MEK is supported by the DFG Research Unit 2239 "New Physics at the LHC". TO has received funding from the German Research Foundation (DFG) under Grant Nos. EXC-1098, FOR 2239 and GRK 1581, and from the European Research Council (ERC) under the European Union's Horizon 2020 research and innovation programme (Grant agreement No. 637506, "νDirections"). TO would also like to thank the CERN Theoretical Physics Department for hospitality and support. FS is supported by the ERC Recognition Award ERC-RA-0008 of the Helmholtz Association.

Funded by SCOAP[3].

Appendix A: Calculation of the mass spectrum at the low scale

The quartic couplings are not free parameters but predicted at the matching scale between the THDM and its UV completion. Therefore, it is necessary to treat them as $\overline{\text{MS}}$ parameters and to perform a calculation of the scalar masses and mixings including the higher order corrections. In practice, we perform the following steps:

1. The running couplings $\lambda_i(Q)$ and $M_{12}(Q)$ at the scale $Q = m_t$ are taken as input, while the SM parameters are evolved to this scale including all known SM corrections, i.e. three-loop running and two-loop matching for g_3 and Y_t.
2. The running VEVs $v_1(Q)$ and $v_2(Q)$ are calculated from:

$$v_1 = \frac{v(Q)}{\sqrt{1+t_\beta^2}}, \tag{A1}$$

$$v_2 = \frac{t_\beta v(Q)}{\sqrt{1+t_\beta^2}}, \tag{A2}$$

where $v(Q)$ is the running VEV and $\tan\beta$ is taken as input which is also defined at $Q = m_t$. The running VEV is

calculated from the gauge couplings and the $\overline{\text{MS}}$ vector boson masses

$$M_V^{\overline{\text{MS}}}(Q) = \sqrt{M_V^2 + \Pi_{VV}^T(M_V^2)}, \tag{A3}$$

where M_V is the pole mass and $\Pi_{VV}^T(M_V^2)$ the $\overline{\text{MS}}$ self energy calculated at the scale Q with external momentum M_V.

3. The tree-level tadpole equations are solved to obtain m_1^2 and m_2^2:

$$T_1 \equiv \frac{\partial V}{\partial \phi_1}\Big|_{\phi_1=v_1} = v_1 m_1^2 + \frac{1}{4}\Big[4v_2 M_{12}^2 + 4\lambda_1 v_1^3 + v_1 v_2^2\Big(2\Big(\lambda_3+\lambda_4\Big)+2\lambda_5\Big)\Big] = 0\,, \tag{A4}$$

$$T_2 \equiv \frac{\partial V}{\partial \phi_2}\Big|_{\phi_2=v_2} = v_2 m_2^2 + \frac{1}{4}\Big[4v_1 M_{12}^2 + 4\lambda_2 v_2^3 + v_2 v_1^2\Big(2\Big(\lambda_3+\lambda_4\Big)+2\lambda_5\Big)\Big] = 0. \tag{A5}$$

4. The tree-level masses are calculated by diagonalising the mass matrices

$$m_h^2 = \begin{pmatrix} \frac{1}{2}\Big(6\lambda_1 v_1^2 + v_2^2\Big(\lambda_3+\lambda_4+\lambda_5\Big)\Big) + m_1^2 & \frac{1}{2}v_1 v_2\Big(2\Big(\lambda_3+\lambda_4\Big)+2\lambda_5\Big) + M_{12}^2 \\ \cdot & \frac{1}{2}\Big(6\lambda_2 v_2^2 + v_1^2\Big(\lambda_3+\lambda_4+\lambda_5\Big)\Big) + m_2^2 \end{pmatrix} \tag{A6}$$

$$m_{A^0}^2 = \begin{pmatrix} \frac{1}{2}\Big(2\lambda_1 v_1^2 + v_2^2\Big(\lambda_3+\lambda_4-\lambda_5\Big)\Big) + m_1^2 & v_1 v_2 \lambda_5 + M_{12}^2 \\ \cdot & \frac{1}{2}\Big(2\lambda_2 v_2^2 + v_1^2\Big(\lambda_3+\lambda_4-\lambda_5\Big)\Big) + m_2^2 \end{pmatrix} + \xi_Z M_Z^2 \tag{A7}$$

$$m_{H^-}^2 = \begin{pmatrix} \frac{1}{2}\lambda_3 v_2^2 + \lambda_1 v_1^2 + m_1^2 & \frac{1}{2}\Big(\lambda_4+\lambda_5\Big)v_1 v_2 + M_{12}^{2*} \\ \cdot & \frac{1}{2}\lambda_3 v_1^2 + \lambda_2 v_2^2 + m_2^2 \end{pmatrix} + \xi_{W^-} M_{W^-}^2 \tag{A8}$$

5. The one- and two-loop corrections δt_i to the tadpoles are calculated. The imposed renormalisation conditions are:

$$T_i + \delta t_i = 0, \quad i = 1, 2, \tag{A9}$$

which cause shifts in the Lagrangian parameters m_i^2:

$$m_i^2 \to m_i^2 + \delta m_i^2, \quad i = 1, 2. \tag{A10}$$

6. The one- and two-loop self-energies for real scalars are calculated for external gauge eigenstates. At the one-loop level, the full dependence on the external momenta is included, while at two-loop, the approximation $p^2 = 0$ as well as the gauge-less limit, i.e. $g_1 = g_2 = 0$, is used. The pole masses are the eigenvalues of the loop-corrected mass matrix calculated as

$$M_\phi^{(2L)}(p^2) = \tilde{M}_\phi^{(2L)} - \Pi_\phi(p^2)^{(1L)} - \Pi_\phi(0)^{(2L)}. \tag{A11}$$

Here, $\tilde{M}_\phi$ is the tree-level mass matrix including the shifts of (A10). Particular care is needed for the two-loop corrections because we work in the gaugeless limit where the Goldstone bosons are massless. Those cause IR divergences in the two-loop integrals. In order to avoid this so called 'Goldstone bosons catastrophe', we use the approach presented in Refs. [51,66].
For charged scalars, the scalar masses are available at the one-loop level,

$$M_\phi^{(1L)}(p^2) = \tilde{M}_\phi^{(1L)} - \Pi_\phi(p^2)^{(1L)}. \tag{A12}$$

The calculation of the one-loop self-energies in both cases is done iteratively for each eigenvalue i until the on-shell condition

$$\Big[\text{eig}M_\phi^{(n)}(p^2 = m_{\phi_i}^2)\Big]_i \equiv m_{\phi_i}^2, \tag{A13}$$

is fulfilled.

References

1. ATLAS Collaboration, G. Aad et al., Observation of a new particle in the search for the Standard Model Higgs boson with the ATLAS detector at the LHC. Phys. Lett. B **716** 1–29 (2012). arXiv:1207.7214
2. C.M.S. Collaboration, S. Chatrchyan, Observation of a new boson at a mass of 125 GeV with the CMS experiment at the LHC. Phys. Lett. B **716**, 30–61 (2012). arXiv:1207.7235
3. LHC Higgs Cross Section Working Group Collaboration, D. de Florian et al., Handbook of LHC Higgs Cross sections: 4. Deciphering the nature of the Higgs Sector. arXiv:1610.07922

4. ATLAS, CMS Collaboration, G. Aad et al., Measurements of the Higgs boson production and decay rates and constraints on its couplings from a combined ATLAS and CMS analysis of the LHC pp collision data at $\sqrt{s} = 7$ and 8 TeV. JHEP **8**, 045 (2016). arXiv:1606.02266
5. G.C. Branco, P.M. Ferreira, L. Lavoura, M.N. Rebelo, M. Sher, J.P. Silva, Theory and phenomenology of two-Higgs-doublet models. Phys. Rept. **516**, 1–102 (2012). arXiv:1106.0034
6. L.D. McLerran, M.E. Shaposhnikov, N. Turok, M.B. Voloshin, Why the baryon asymmetry of the universe is approximately 10**-10. Phys. Lett. B **256**, 451–456 (1991)
7. N. Turok, J. Zadrozny, Electroweak baryogenesis in the two doublet model. Nucl. Phys. B **358**, 471–493 (1991)
8. A.G. Cohen, D.B. Kaplan, A.E. Nelson, Spontaneous baryogenesis at the weak phase transition. Phys. Lett. B **263**, 86–92 (1991)
9. V. Zarikas, The Phase transition of the two Higgs extension of the standard model. Phys. Lett. B **384**, 180–184 (1996). arXiv:hep-ph/9509338
10. J.M. Cline, P.-A. Lemieux, Electroweak phase transition in two Higgs doublet models. Phys. Rev. D **55**, 3873–3881 (1997). arXiv:hep-ph/9609240
11. L. Fromme, S.J. Huber, M. Seniuch, Baryogenesis in the two-Higgs doublet model. JHEP **11**, 038 (2006). arXiv:hep-ph/0605242
12. G.C. Dorsch, S.J. Huber, K. Mimasu, J.M. No, The Higgs vacuum uplifted: revisiting the electroweak phase transition with a second Higgs doublet. JHEP **12**, 086 (2017). arXiv:1705.09186
13. P. Basler, M. Krause, M. Muhlleitner, J. Wittbrodt, A. Wlotzka, Strong first order electroweak phase transition in the CP-conserving 2HDM revisited. JHEP **02**, 121 (2017). arXiv:1612.04086
14. G .C. Dorsch, S .J. Huber, K. Mimasu, J .M. No, Hierarchical versus degenerate 2HDM: The LHC run 1 legacy at the onset of run 2. Phys. Rev. **D93**(11), 115033 (2016). arXiv:1601.04545
15. G .C. Dorsch, S .J. Huber, K. Mimasu, J .M. No, Echoes of the electroweak phase transition: discovering a second Higgs doublet through $A_0 \to ZH_0$. Phys. Rev. Lett. **113**(21), 211802 (2014). arXiv:1405.5537
16. G.C. Dorsch, S.J. Huber, J.M. No, A strong electroweak phase transition in the 2HDM after LHC8. JHEP **10**, 029 (2013). arXiv:1305.6610
17. N. Chakrabarty, U.K. Dey, B. Mukhopadhyaya, High-scale validity of a two-Higgs doublet scenario: a study including LHC data. JHEP **12**, 166 (2014). arXiv:1407.2145
18. N. Chakrabarty, B. Mukhopadhyaya, High-scale validity of a two Higgs doublet scenario: metastability included. Eur. Phys. J. **C77**(3), 153 (2017). arXiv:1603.05883
19. P. Ferreira, H.E. Haber, E. Santos, Preserving the validity of the Two-Higgs Doublet Model up to the Planck scale. Phys. Rev. D **92**, 033003 (2015). arXiv:1505.04001. [Erratum: Phys. Rev. D94, no.5,059903(2016)]
20. N. Chakrabarty, B. Mukhopadhyaya, High-scale validity of a two Higgs doublet scenario: predicting collider signals. Phys. Rev **D96**(3), 035028 (2017). arXiv:1702.08268
21. D. Chowdhury, O. Eberhardt, Global fits of the two-loop renormalized Two-Higgs-Doublet model with soft Z_2 breaking. JHEP **11**, 052 (2015). arXiv:1503.08216
22. P. Basler, P.M. Ferreira, M. Mühlleitner, R. Santos, High scale impact in alignment and decoupling in two-Higgs doublet models. Phys. Rev. **D97**(9), 095024 (2018). arXiv:1710.10410
23. H.E. Haber, R. Hempfling, The Renormalization group improved Higgs sector of the minimal supersymmetric model. Phys. Rev. D **48**, 4280–4309 (1993). arXiv:hep-ph/9307201
24. M. Gorbahn, S. Jager, U. Nierste, S. Trine, The supersymmetric Higgs sector and $B - \bar{B}$ mixing for large tan β. Phys. Rev. D **84**, 034030 (2011). arXiv:0901.2065
25. G. Lee, C .E .M. Wagner, Higgs bosons in heavy supersymmetry with an intermediate m_A. Phys. Rev. **D92**(7), 075032 (2015). arXiv:1508.00576
26. H. Bahl, W. Hollik, Precise prediction of the MSSM Higgs boson masses for low MA. arXiv:1805.00867
27. J. Mrazek, A. Pomarol, R. Rattazzi, M. Redi, J. Serra, A. Wulzer, The other natural two Higgs doublet model. Nucl. Phys. B **853**, 1–48 (2011). arXiv:1105.5403
28. L. Zarate, The Higgs mass and the scale of SUSY breaking in the NMSSM. JHEP **07**, 102 (2016). arXiv:1601.05946
29. A. Barroso, P.M. Ferreira, I.P. Ivanov, R. Santos, Metastability bounds on the two Higgs doublet model. JHEP **06**, 045 (2013). arXiv:1303.5098
30. J. Braathen, M.D. Goodsell, M.E. Krauss, T. Opferkuch, F. Staub, N-loop running should be combined with N-loop matching. Phys. Rev. **D97**(1), 015011 (2018). arXiv:1711.08460
31. H.S. Cheon, S.K. Kang, Constraining parameter space in type-II two-Higgs doublet model in light of a 126 GeV Higgs boson. JHEP **09**, 085 (2013). arXiv:1207.1083
32. S. Gori, H.E. Haber, E. Santos, High scale flavor alignment in two-Higgs doublet models and its phenomenology. JHEP **06**, 110 (2017). arXiv:1703.05873
33. P.S. BhupalDev, A. Pilaftsis, Maximally symmetric two Higgs doublet model with natural standard model alignment. JHEP **12**, 24 (2014). arXiv:1408.3405. [Erratum: JHEP11,147(2015)]
34. D. Das, I. Saha, Search for a stable alignment limit in two-Higgs-doublet models. Phys. Rev. D **91**(9), 095024 (2015). arXiv:1503.02135
35. M.D. Goodsell, F. Staub, Improved unitarity constraints in Two-Higgs-Doublet-Models. Phys. Lett. B **788**, 206–212 (2019). https://doi.org/10.1016/j.physletb.2018.11.030
36. H.E. Haber, G.L. Kane, The search for supersymmetry: probing physics beyond the standard model. Phys. Rept. **117**, 75–263 (1985)
37. M. Gabelmann, M. Mühlleitner,, F. Staub, Automatised matching between two scalar sectors at the one-loop level (2018). arXiv:1810.12326
38. S. Kanemura, T. Kubota, E. Takasugi, Lee-Quigg-Thacker bounds for Higgs boson masses in a two doublet model. Phys. Lett. B **313**, 155–160 (1993). arXiv:hep-ph/9303263
39. A.G. Akeroyd, A. Arhrib, E.-M. Naimi, Note on tree level unitarity in the general two Higgs doublet model. Phys. Lett. B **490**, 119–124 (2000). arXiv:hep-ph/0006035
40. F. Staub, SARAH. arXiv:0806.0538
41. F. Staub, From superpotential to model files for FeynArts and CalcHep/CompHep. Comput. Phys. Commun. **181**, 1077–1086 (2010). arXiv:0909.2863
42. F. Staub, Automatic calculation of supersymmetric renormalization group equations and self energies. Comput. Phys. Commun. **182**, 808–833 (2011). arXiv:1002.0840
43. F. Staub, SARAH 3.2: Dirac Gauginos, UFO output, and more. Comput. Phys. Commun. **184**, 1792–1809 (2013). https://doi.org/10.1016/j.cpc.2013.02.019
44. F. Staub, SARAH 4: A tool for (not only SUSY) model builders. Comput. Phys. Commun. **185**, 1773–1790 (2014). arXiv:1309.7223
45. F. Staub, Exploring new models in all detail with SARAH. Adv. High Energy Phys. **2015**, 840780 (2015). arXiv:1503.04200
46. W. Porod, SPheno, a program for calculating supersymmetric spectra, SUSY particle decays and SUSY particle production at e+ e- colliders. Comput. Phys. Commun. **153**, 275–315 (2003). arXiv:hep-ph/0301101
47. W. Porod, F. Staub, SPheno 3.1: Extensions including flavour, CP-phases and models beyond the MSSM. Comput. Phys. Commun. **183**, 2458–2469 (2012). https://doi.org/10.1016/j.cpc.2012.05.021

48. F. Staub, W. Porod, Improved predictions for intermediate and heavy supersymmetry in the MSSM and beyond. Eur. Phys. J. **C77**(5), 338 (2017). arXiv:1703.03267
49. M.D. Goodsell, K. Nickel, F. Staub, Two-Loop Higgs mass calculations in supersymmetric models beyond the MSSM with SARAH and SPheno. Eur. Phys. J. C **75**(1), 32 (2015). arXiv:1411.0675
50. M. Goodsell, K. Nickel, F. Staub, Generic two-loop Higgs mass calculation from a diagrammatic approach. Eur. Phys. J. C **75**(6), 290 (2015). arXiv:1503.03098
51. J. Braathen, M.D. Goodsell, F. Staub, Supersymmetric and non-supersymmetric models without catastrophic Goldstone bosons. Eur. Phys. J. C **77**(11), 757 (2017). arXiv:1706.05372
52. K.S. Babu, R.N. Mohapatra, Minimal supersymmetric left-right model. Phys. Lett. B **668**, 404–409 (2008). arXiv:0807.0481
53. L. Basso, B. Fuks, M.E. Krauss, W. Porod, Doubly-charged Higgs and vacuum stability in left-right supersymmetry. JHEP **07**, 147 (2015). arXiv:1503.08211
54. M.E. Krauss, F. Staub, Perturbativity constraints in BSM models. Eur. Phys. J. C **78**(3), 185 (2018). arXiv:1709.03501
55. F. Staub, Reopen parameter regions in Two-Higgs Doublet models. Phys. Lett. B **776**, 407–411 (2018). arXiv:1705.03677
56. J.E. Camargo-Molina, B. O'Leary, W. Porod, F. Staub, Vevacious: a tool for finding the global minima of one-loop effective potentials with many scalars. Eur. Phys. J. C **73**(10), 2588 (2013). arXiv:1307.1477
57. T. Lee, T. Li, C. Tsai, Hom4ps-2.0: a software package for solving polynomial systems by the polyhedral homotopy continuation method. Computing **83**(2), 109–133 (2008)
58. S.R. Coleman, E.J. Weinberg, Radiative corrections as the origin of spontaneous symmetry breaking. Phys. Rev. D **7**, 1888–1910 (1973)
59. J.R. Espinosa, G.F. Giudice, E. Morgante, A. Riotto, L. Senatore, A. Strumia, N. Tetradis, The cosmological Higgstory of the vacuum instability. JHEP **09**, 174 (2015). arXiv:1505.04825
60. A. Hook, J. Kearney, B. Shakya, K.M. Zurek, Probable or improbable universe? Correlating electroweak vacuum instability with the scale of inflation. JHEP **01**, 061 (2015). arXiv:1404.5953
61. P. Bechtle, O. Brein, S. Heinemeyer, G. Weiglein, K.E. Williams, HiggsBounds: confronting arbitrary Higgs sectors with exclusion bounds from LEP and the tevatron. Comput. Phys. Commun. **181**, 138–167 (2010). arXiv:0811.4169
62. P. Bechtle, O. Brein, S. Heinemeyer, O. Stål, T. Stefaniak, G. Weiglein, K.E. Williams, HiggsBounds—4: improved tests of extended Higgs Sectors against exclusion bounds from LEP, the tevatron and the LHC. Eur. Phys. J. C **74**(3), 2693 (2014). arXiv:1311.0055
63. M. Misiak, M. Steinhauser, Weak radiative decays of the B meson and bounds on $M_{H^\pm}$ in the Two-Higgs-Doublet Model. Eur. Phys. J. C **77**(3), 201 (2017). arXiv:1702.04571
64. W. Porod, F. Staub, A. Vicente, A Flavor Kit for BSM models. Eur. Phys. J. C **74**(8), 2992 (2014). arXiv:1405.1434
65. N.G. Deshpande, E. Ma, Pattern of symmetry breaking with two Higgs doublets. Phys. Rev. D **18**, 2574 (1978)
66. J. Braathen, M.D. Goodsell, Avoiding the Goldstone Boson Catastrophe in general renormalisable field theories at two loops. JHEP **12**, 056 (2016). arXiv:1609.06977